

1 **Direct observations indicate photodegradable oxygenated VOCs**
2 **as larger contributors to radicals and ozone production in the**
3 **atmosphere**

4 Wenjie Wang^{1,2}, Bin Yuan^{1,3*}, Yuwen Peng^{1,3}, Hang Su^{2*}, Yafang Cheng², Suxia Yang^{1,3},
5 Caihong Wu^{1,3}, Jipeng Qi^{1,3}, Fengxia Bao², Yibo Huangfu^{1,3}, Chaomin Wang^{1,3},
6 Chenshuo Ye¹, Zelong Wang^{1,3}, Baolin Wang⁴, Xinming Wang⁵, Wei Song⁵, Weiwei
7 Hu⁵, Peng Cheng⁶, Manni Zhu^{1,3}, Junyu Zheng^{1,3}, Min Shao^{1,3}

8
9 ¹ Institute for Environmental and Climate Research, Jinan University,
10 Guangzhou 511443, China

11 ² Multiphase Chemistry Department, Max Planck Institute for Chemistry, Mainz
12 55128, Germany.

13 ³ Guangdong-Hongkong-Macau Joint Laboratory of Collaborative Innovation for
14 Environmental Quality, Guangzhou, 511443, China

15 ⁴ School of Environmental Science and Engineering, Qilu University of
16 Technology, Jinan 250353, China

17 ⁵ State Key Laboratory of Organic Geochemistry, Guangzhou Institute of
18 Geochemistry, Chinese Academy of Sciences, Guangzhou 510640, China

19 ⁶ Institute of Mass Spectrometry and Atmospheric Environment, Jinan
20 University, Guangzhou 510632, China

21

22 **Correspondence to:* Bin Yuan (byuan@jnu.edu.cn); Hang Su (h.su@mpic.de)

23

24

25 **Abstract:** Volatile organic compounds (VOCs) regulate atmospheric oxidation capacity,
26 and the reactions of VOCs are key in understanding ozone formation and its mitigation
27 strategies. When evaluating their impact, most previous studies did not fully consider
28 the role of oxygenated VOCs due to limitations of measurement technology. By using
29 a proton-transfer-reaction time-of-flight mass spectrometer (PTR-ToF-MS) combined
30 with a gas chromatography mass spectrometer (GC-MS), a large number of oxygenated
31 VOCs have been quantified in Guangzhou city, China. Based on the new dataset, we
32 demonstrate that constraints using OVOCs observations are essential in modeling
33 radical and ozone production, as modelled OVOCs can be substantially lower than
34 measurements, potentially due to primary emissions and/or missing secondary sources.
35 Non-formaldehyde (HCHO) OVOCs can contribute large fractions (22-44%) of total
36 RO_x radical production, which are comparable to or larger than the contributions from
37 nitrous acid and formaldehyde. Our results show that models without OVOC
38 constraints using ambient measurements will underestimate the production rates of
39 RO_x and ozone, and may also affect the determination of sensitivity regime in ozone
40 formation. Therefore, a thorough quantification of photodegradable OVOCs species is
41 in urgent need to understand accurately the ozone chemistry and to develop effective
42 control strategies.

43

44 **Keywords:** photolysis reactions; oxygenated volatile organic compounds; radical
45 production; ozone production

46

47 **1 Introduction**

48 Ground-level ozone is generated by photochemical oxidation of volatile organic
49 compounds (VOCs) under the catalysis of nitrogen oxides (NO_x) and hydrogen oxide
50 radicals (HO_x=OH+HO₂) (Atkinson, 2000;Monks et al., 2015). In this process,
51 photolysis reactions are a crucial driving force (Wang et al., 2019). Photolysis of O₃,
52 nitrous acid (HONO), and oxygenated VOCs (OVOCs) can contribute to primary
53 production of RO_x (OH+HO₂+RO₂) radicals, thereby accelerating the recycling of
54 radicals to generate ozone (Volkamer et al., 2010). The strong dependence of OH
55 concentration on $j(\text{O}^1\text{D})$ was found in a number of field measurements (Ehhalt and
56 Rohrer, 2000;Rohrer et al., 2014b;Stone et al., 2012), implying the dominant role of
57 ultraviolet radiation and photolysis reactions in the production of HO_x radicals.
58 Edwards et al. (2014) found that the high ozone pollution in an oil and gas producing
59 basin in the U.S. in winter was caused by the photolysis of high concentrations of
60 OVOCs to generate sufficient oxidants. A recent model simulation with limited
61 OVOCs measurements by Qu et al.(Qu et al., 2021) indicated that OVOC species are
62 the largest free-radical source in the boundary layer. Another study indicated that fast
63 ozone production during winter haze episodes in China was driven by HO_x radicals
64 derived from photolysis of formaldehyde (HCHO), overcoming radical titration
65 induced by NO_x emissions (Li et al., 2021). Furthermore, high loading of aerosols can
66 largely influence the production of radicals and ozone through altering photolysis
67 reaction rate (Wang et al., 2019;Wang et al., 2020b;Wang et al., 2021a). Therefore, an
68 accurate quantification of numerous photolysis reactions is necessary to understand
69 the mechanism of RO_x radical and ozone production.

70 However, only limited number of photodegradable OVOC species, such as
71 formaldehyde, acetaldehyde and acetone, have been measured in the field campaigns
72 in China due to the limitations on available instrumentation(Lu et al., 2013;Lu et al.,
73 2012;Tan et al., 2018;Tan et al., 2019c). Many important photodegradable OVOCs,
74 such as larger aldehydes and ketones, carboxylic acids, nitrophenols, organic peroxides
75 and multifunctional species, have been rarely quantified accurately in ambient

76 environments. In such cases, the quantification of the primary production of RO_x
77 radicals induced by photolysis reactions may not be adequately accurate. Many studies
78 used photochemical models to simulate unmeasured OVOC species (Tan et al.,
79 2019b; Volkamer et al., 2010; Ling et al., 2014; Edwards et al., 2014). However, large
80 uncertainties in the simulation of OVOCs remain due to primary emissions of OVOCs
81 (McDonald et al., 2018; Karl et al., 2018; Gkatzelis et al., 2021), missing secondary
82 sources (Bloss et al., 2005; Ji et al., 2017), heterogenous uptake on aerosols and
83 unknown dilution and transmission processes (Li et al., 2014). For instance, chamber
84 experiments of the oxidation of aromatics by OH radical indicated that MCM
85 mechanism generally underestimated the formation of aldehydes, ketones and phenols
86 by 10-70% (Bloss et al., 2005; Ji et al., 2017), implying the existence of unknown
87 production pathways for these OVOC species. Furthermore, model simulations
88 frequently underestimated observed RO_x radicals in ambient studies of RO_x radicals
89 (Hofzumahaus et al., 2009; Tan et al., 2018; Lelieveld et al., 2008; Rohrer et al.,
90 2014a; Sheehy et al., 2010; Emmerson et al., 2005; Ma et al., 2019). Given that only
91 limited photodegradable OVOC species were measured in these studies, the lack of
92 comprehensive measurements of OVOCs to constrain the model is likely to be a cause
93 of the underestimation.

94 Thus far, the concrete effects of photodegradable OVOCs on radical and ozone
95 production remains unexplored in China. Based on comprehensive field observations
96 in a mega-city in southern China, a variety of important photodegradable OVOC
97 species were measured. The contributions of these photodegradable OVOC species to
98 the production of RO_x radicals are quantified, and the effect of photolysis reactions
99 on ozone production is quantitatively assessed.

100 **2 Materials and Methods**

101 **2.1 OVOC measurements**

102 Field measurements were conducted at an urban site in Guangzhou (113.2°E, 23°N)
103 from 14 September to 20 November 2018. The sampling site is located on the 9th floor

104 of a building on the campus of Guangzhou Institute of Geochemistry, Chinese Academy
105 of Sciences, 25 m above the ground level. This site is regarded as a typical urban site
106 in Guangzhou influenced by industrial and vehicle emissions.

107 During this campaign, an online PTR-ToF-MS (Ionicon Analytic GmbH,
108 Innsbruck, Austria) with H_3O^+ and NO^+ chemistry was used to measure ambient volatile
109 organic compounds (VOCs) (Wang et al., 2020a; Wu et al., 2020). The PTR-ToF-MS
110 automatically switches between H_3O^+ and NO^+ modes every 10-20 minutes. In each
111 mode, the background and ambient measurements were automatically switched to a
112 custom-built Platinum catalytic converter heated to 365 °C for 3 minutes to determine
113 the background of the instrument. The time resolution of the measurement of PTR-ToF
114 -MS was 10 s. A total of 31 VOCs species were calibrated using either gas cylinders or
115 liquid standards. For other measured VOCs, we used the method proposed by Sekimoto
116 et al. (2017) to determine the relationship between VOC sensitivity and kinetic rate
117 constants for proton transfer reactions of H_3O^+ with VOCs. The fitted line was used to
118 determine the concentrations of those uncalibrated species. Following the discussions
119 in Sekimoto, et al. (Sekimoto et al., 2017), the uncertainties of the concentrations for
120 uncalibrated species were about 50 %. Humidity dependencies of various VOCs were
121 determined in the laboratory with absolute humidity in the range of 0–30 mmol/mol
122 (relative humidity of 0 %–92 % at 25 °C), which fully covered the humidity range
123 encountered during the entire campaign. The detailed introduction of this method has
124 been reported by Wu et al. (Wu et al., 2020).

125 Notably, PTR-ToF-MS is not capable of distinguishing isomers (Yuan et al., 2017).
126 GC-MS technique was used to measure several carbonyls that PTR-ToF-MS cannot
127 distinguish, including acetaldehyde, propionaldehyde, n-butanal, n-pentanal, n-hexanal,
128 methacrolein (MACR), methyl vinyl ketone (MVK). We compared concentrations of
129 common OVOC species measured by both GC-MS and PTR-ToF-MS. The agreement
130 of measurement results from the two instruments are quite consistent (Figure S1). In
131 addition to GC-MS, an iodide time-of flight chemical ionization mass spectrometer
132 (ToF-CIMS) was used to measure propionic acid. Combined with the measurements of
133 GC-MS and CIMS, the isomers measured by PTR-ToF-MS can be distinguished. In

134 OVOC species, hydroxyacetone and propionic acid ($C_3H_6O_2$), acetone and propanal
135 (C_3H_6O), methyl ethyl ketone and butanal (C_4H_8O), MVK and MACR (C_4H_6O) are all
136 isomers. The average concentration of propionic acid measured by CIMS was 0.23 ppb,
137 significantly lower than the concentration of $C_3H_6O_2$ measured by PTR-ToF-MS (~1.5
138 ppb). The hydroxyacetone concentrations were determined by the difference between
139 PTR-ToF-MS and CIMS measurements. Meanwhile, the concentration of propanal
140 (average of 0.35 ppb) and n-butanal (average of 0.17 ppb) measured by GC-MS were
141 also respectively far lower than the concentration of C_3H_6O (average of 4.4 ppb) and
142 C_4H_8O (average of 1.8 ppb) measured by PTR-ToF-MS. The concentrations of acetone
143 and methyl ethyl ketone were determined by the difference between PTR-ToF-MS and
144 GC-MS measurements. The concentrations of MVK and MACR were determined
145 according to C_4H_6O concentration measured by PTR-ToF-MS and the ratio of MVK to
146 MACR measured by GC-MS. In this way, the uncertainty of PTR-ToF-MS induced by
147 isomers is greatly reduced.

148 Concentrations of CH_4O_2 and CH_4O_3 were quantified by PTR-ToF-MS, which
149 were tentatively attributed to methyl hydroperoxide (CH_3OOH) and hydroxymethyl
150 hydroperoxide ($HOCH_2OOH$), respectively. Furthermore, concentrations of several
151 small carbon-number acids, including formic acid, acetic acid, and propionic acid were
152 measured by PTR-ToF-MS (**Figure S1**). However, the photolysis wavelength bands of
153 these species are all less than 260 nm. Given the sunlight that can reach the ground is
154 generally greater than 290 nm, these small carbon-number acids cannot photolyze
155 significantly near the ground. An exception is pyruvic acid which is also a small carbon-
156 number acid but with a wide photolysis band that can reach 460 nm because of its
157 additional carbonyl functional group (Horowitz et al., 2001; Mellouki and Mu,
158 2003; Berges and Warneck, 1992). Therefore, the photolysis of pyruvic acid was
159 included in the analysis as it can significantly contribute to the production of RO_x
160 radicals.

161 In addition to the specific species mentioned above, PTR-ToF-MS measured
162 carbonyls with higher carbon number including $C_nH_{2n}O$ ($n>5$), $C_nH_{2n-2}O$ ($n>3$), C_nH_{2n-}
163 $2O_2$ ($n>3$), $C_nH_{2n-4}O_2$ ($n>3$) and $C_nH_{2n-4}O_3$ ($n>3$). Apparently, multiple isomers that

164 can't be distinguished specifically may contribute to these species. The measured
165 photodegradable OVOCs species and their concentrations are summarized in **Table S1**.

166 **2.2 Other measurements**

167 HONO was measured by a custom-built LOPAP (L^Ong Path Absorption
168 Photometer) based on wet chemical sampling and photometric detection (Yu et al.,
169 2021). HCHO was measured by a custom-built instrument based on the Hantzsch
170 reaction and absorption photometry. Total OH reactivity was measured by the
171 comparative reactivity method (CRM) (Sinha et al., 2008; Wang et al., 2021b). In this
172 method, pyrrole (C₄H₅N) was used as the reference substance and was quantified by a
173 quadrupole PTR-MS (Ionicon Analytic, Austria). Non-methane hydrocarbons
174 (NMHCs) were measured using a gas chromatography-mass spectrometer/flame
175 ionization detector (GC-MS/FID) system, coupled with a cryogen-free pre-
176 concentration device. Nitrogen oxides (NO_x= NO + NO₂), ozone (O₃), sulfur dioxide
177 (SO₂) and carbon monoxide (CO) were measured by NO_x analyzer (Thermo
178 Scientific, Model 42i), O₃ analyzer (Thermo Scientific, 150 Model 49i), SO₂ analyzer
179 (Thermo Scientific, Model 43i) and CO analyzer (Thermo Scientific, Model 48i). The
180 meteorological data, including temperature (T), relative humidity (RH) and wind
181 speed and direction 160 (WS, WD) were recorded by Vantage Pro2 Weather Station
182 (Davis Instruments Inc., Vantage Pro2) with the time resolution of 1 min. Photolysis
183 frequencies including j(HONO), j(NO₂), j(H₂O₂), j(HCHO) and j(O¹D) were
184 measured by a spectrometer (Focused Photonics Inc., PFS-100).

185 **2.3 Observation-based box model**

186 A zero-dimensional box model coupled with the Master Chemical Mechanism
187 (MCM) v3.3.1 chemical mechanism (Jenkin et al., 2003; Saunders et al., 2003) was
188 used to simulate RO_x production and losses, and O₃ production rates during the field
189 campaign. The model simulation was constrained to the observations of
190 meteorological parameters, photolysis frequencies, and concentrations of non-
191 methane hydrocarbons (NMHCs), OVOCs, NO, NO₂, O₃, CO, SO₂ and nitrous acid

192 (HONO). All constraints were averaged to generate a synchronized 1-h time
 193 resolution dataset. The model runs were performed in a time-dependent mode with
 194 time resolution of 1 hour and spin-up of two days. There is no significant difference in
 195 simulated OH and HO₂ concentrations between 1-hour and 5-minute time resolution
 196 (Figure S3). A 24-h lifetime was introduced for all simulated species, including
 197 secondary species and radicals, to approximately simulate dry deposition and other
 198 losses of these species (Lu et al., 2013; Wang et al., 2020c). Sensitivity tests show that
 199 this assumed physical loss lifetime has a relatively small influence on the reactivity of
 200 modeled oxidation products, RO_x radicals and ozone production rates. A 50% change
 201 in the physical loss lifetime leads to 3%, 6% and 10% changes in OH concentration,
 202 HO₂ concentration and ozone production rate. The ozone production rate (P(O₃)) were
 203 calculated according to E1:

$$204 \quad P(O_3) = k_{HO_2+NO}[HO_2][NO] + \sum_i(k_{RO_2+NO}^i [RO_2^i][NO]) \quad E1$$

205 The production rate of RO_x radicals (P(RO_x)) is equal to the sum of the rates at
 206 which all photodegradable species generate RO_x radicals through the photolysis
 207 reactions, as shown in E2.

$$208 \quad P(RO_x) = 2 \times [O_3] \times j(O^1D) \times \theta + [HONO] \times j(HONO) + \sum_i[OVOC_i] \times j_i \times k_i \quad E2$$

209 where θ is the fraction of O¹D from ozone photolysis that reacts with water vapor.
 210 OVOC_i represents each OVOC species, j_i represents the photolysis frequency of each
 211 OVOC species, and k_i represents the number of RO_x radicals generated from the
 212 photolysis of each OVOC molecule. For most OVOC species, k_i is equal to 2 or 1.

213 The photolysis frequencies of measured photodegradable species were calculated
 214 based on measured actinic flux combined with absorption cross sections and
 215 photolysis quantum yields reported in Jet Propulsion Laboratory (JPL) publication
 216 (Burkholder et al., 2020). Note that absorption cross sections and quantum yields used
 217 all correspond to radical formation channels, and do not include contributions from
 218 channels forming stable molecules. However, absorption cross sections and photolysis
 219 quantum yields for nitrophenol and methyl nitrophenol are unavailable from JPL
 220 publication. Yuan et al. (2016) have reported that photolysis was the most efficient

221 loss pathway for nitrophenol in the gas phase. Different values of absorption cross
222 sections and quantum yields for nitrophenol have been reported (Chen et al.,
223 2011; Sangwan and Zhu, 2018; Bejan et al., 2006). In this study, we used the values
224 from Chen et al. (Chen et al., 2011), which can reproduce well the observed
225 concentrations of nitrophenol and methyl nitrophenol during the measurement period.

226 Absorption cross sections and quantum yields are not available for carbonyls
227 with large carbon number, and absorption cross sections and quantum yields of
228 species with similar structure are used as a surrogate, following the method described
229 in Jenkin et al., (Jenkin et al., 1997) (e.g. $C_2H_5C(O)CH_3$ is used as a surrogate for
230 aliphatic ketones with more carbons). Another issue is that carbonyls with large
231 carbon number ($C_nH_{2n}O$, $n>5$; $C_nH_{2n-2}O$, $n>3$; $C_nH_{2n-2}O_2$, $n>3$; $C_nH_{2n-4}O_2$, $n>3$; $C_nH_{2n-4}O_3$, $n>3$) measured by PTR-ToF-MS may include contributions from multiple
232 isomers, and the fraction of each individual species cannot be obtained. Hence, each
233 molecular formula corresponds to multiple molecular structures and thus corresponds
234 to multiple photolysis frequencies. Here, we calculate the $P(RO_x)$ of these species in
235 two scenarios: (1) each molecular formula corresponds to minimum photolysis
236 frequency of all potential species (e.g. aliphatic ketones); (2) each molecular formula
237 corresponds to maximum photolysis frequency of all potential species (e.g.
238 aldehydes). As a result, photolysis frequencies of these carbonyls with large carbon
239 number were assigned to the ranges of $1.2 \times 10^{-6} \sim 6.5 \times 10^{-6}$, $1.2 \times 10^{-6} \sim 6.5 \times 10^{-6}$, 1.2×10^{-6}
240 $\sim 1.2 \times 10^{-4}$, $1.2 \times 10^{-6} \sim 3.0 \times 10^{-4}$ and $1.2 \times 10^{-6} \sim 1.8 \times 10^{-4} \text{ s}^{-1}$, respectively (Jenkin et al.,
241 1997) (**Table S1**). The lowest and highest values of these photolysis frequencies were
242 separately used to determine the lower and upper limits of $P(RO_x)$. Therefore, the
243 total $P(RO_x)$ contributed by all these OVOC species could be investigated.

245 **3 Results and discussion**

246 **3.1 Overview of the observations**

247 During the observation period, we used PTR-ToF-MS and GC-MS instruments to
248 measure more than 20 photodegradable OVOC species. The concentrations and

249 photolysis frequencies of measured photodegradable OVOC species are summarized in
250 **Table S1 and Figure 1**. Previous studies have reported that these species have
251 relatively large absorption cross section and quantum yield (Burkholder et al., 2020).
252 The measured daytime average photolysis frequencies for these species were generally
253 larger than $1.3 \times 10^{-6} \text{ s}^{-1}$.

254 **Figure 1** presents the average diurnal variation of photodegradable OVOC species
255 during the measurement period. The concentrations of these species ranged from 0.01
256 to 10 ppb. HCHO, methylglyoxal, propionaldehyde, n-butanal, n-pentanal,
257 MVK+MACR, pyruvic acid, formic acid, acetic acid, and CH_3OOH had similar diurnal
258 variation patterns. The concentrations of these species started to increase from about
259 6:00 in the morning, and peaked at 13:00-16:00, after which the concentrations
260 gradually decreased. This diurnal variation pattern is a typical secondary production
261 pattern, and thus we deduce that these species primarily came from secondary
262 production. Acetaldehyde, acetone and acrolein showed diurnal variations without
263 significant variations throughout the day, as these species were contributed to by both
264 secondary generation and primary emissions or background contribution (Wu et al.,
265 2020). It is notable that acrolein, nitrophenol and methylnitrophenol all peaked at 20:00
266 in the evening, which is likely due to primary emissions e.g. biomass burning due to
267 wild/agricultural fires (Ye et al., 2021) and vehicle emissions.

268 The ratio of secondary OVOCs to NMHCs can characterize the degree of the
269 conversion of emitted NMHC to secondary OVOCs through oxidation reactions.
270 **Figure S4** presents the correlation between daily daytime average of HCHO (and
271 pyruvic acid) concentration versus OH reactivity from hydrocarbons, i.e.,
272 $\text{HCHO}/\text{R}_{\text{OH_NMHC}}$ ratio (and pyruvic acid/ $\text{R}_{\text{OH_NMHC}}$ ratio) and $j(\text{NO}_2)$. Both
273 $\text{HCHO}/\text{R}_{\text{OH_NMHC}}$ and pyruvic acid/ $\text{R}_{\text{OH_NMHC}}$ ratios displayed significant positive
274 correlation with $j(\text{NO}_2)$. These results suggest that the enhancement of the photolysis
275 rates converted more NMHCs into secondary OVOCs, suggesting the crucial role of
276 photolysis reactions in the air mass aging and the occurrence of secondary pollution.

277 3.2 Contribution of photolysis reactions to the production of RO_x radicals

278 The photolysis of O₃, HONO and OVOCs are the most important contributors to
279 the production of RO_x radicals. All observed photodegradable species, including O₃,
280 HONO and OVOCs, were constrained in the box model to calculate P(RO_x). The
281 simulated total P(RO_x) contains the contributions from all observed photodegradable
282 species and several simulated OVOCs that was not measured such as glyoxal. Using
283 the possible ranges of photolysis frequencies of carbonyls with larger carbon number
284 that are not possible to assign into specific individual species, we can obtain the possible
285 widest variation range of P(RO_x). As shown in **Figure 2a**, the minimum (solid line)
286 and maximum (dashed line) of P(RO_x) calculated during the campaign peaked at 3.6
287 ppb h⁻¹ and 5.4 ppb h⁻¹, respectively. The P(RO_x) determined in this study is very close
288 to those reported in the Autumn 2014 in Pearl River Delta with peak values of 3 ~ 4
289 ppb h⁻¹ (Tan et al., 2019a) and the summer 2014 in Wangdu, Hebei (peak value of 5 ppb
290 h⁻¹) (Tan et al., 2017), and lower than those in the summer 2006 in Beijing (peak value
291 of about 7 ppb h⁻¹) (Lu et al., 2013) and the summer 2006 in Guangzhou (peak value of
292 about 10 ppb h⁻¹) (Lu et al., 2012), and higher than those in the winter of 2016 in Beijing
293 (peak value of about 1 ppb h⁻¹) (Tan et al., 2018) and the winter in the oil and gas basin
294 of Utah, USA (daytime average value of 0.77 ppb h⁻¹) (Edwards et al., 2014). Note that
295 these previous studies mentioned above usually only measured a few simple carbonyls
296 such as HCHO, acetaldehyde and acetone and the P(RO_x) contributed by photolysis of
297 other OVOCs was calculated by model simulations, which may lead to large
298 uncertainties, due to various possibility in modelling errors, including missing primary
299 emissions of OVOCs (McDonald et al., 2018), unknown secondary sources of OVOCs
300 (Bloss et al., 2005; Ji et al., 2017), heterogenous uptake on aerosols and unknown
301 dilution and transport processes (Li et al., 2014).

302 For the scenario of minimum OVOCs contribution, HONO contributed the most
303 to P(RO_x) (37%), followed by O₃ (20%) and HCHO (20%). The contribution of non-
304 HCHO OVOCs was 21% (**Figure 2a**). Figure 2b and Figure S5 show the relative
305 contributions of different non-HCHO OVOC species to P(RO_x) for the scenarios with

306 minimum and maximum OVOC contribution, respectively. Ozonolysis of alkenes
307 played a minor role in P(RO_x). For the scenario of maximum OVOCs contribution, the
308 contribution of non-HCHO OVOCs increased to 44%. In total, OVOCs contributed 43%
309 ~ 59% of P(RO_x), which is higher than previous studies that reported that OVOCs
310 contributed 17%~40% of P(RO_x) in major cities in China and the US (Tan et al.,
311 2019a;Tan et al., 2017;Tan et al., 2018;Tan et al., 2019b;Young et al., 2012;Griffith et
312 al., 2016). In this study the contribution of OVOCs to P(RO_x) was higher than that of
313 HONO. This is different from previous studies reporting HONO contributed more to
314 P(RO_x) than OVOCs in China (Tan et al., 2019a;Tan et al., 2017;Tan et al., 2018;Tan
315 et al., 2019b). Nevertheless, it is notable that the contributions of HONO to P(RO_x) in
316 the early morning were higher than those of OVOCs due to the accumulation of HONO
317 in nighttime, while OVOCs dominate P(RO_x) at noon when photochemistry was most
318 active (**Figure 2a**). Furthermore, those previous studies in China indicated that HCHO
319 was the dominant contributor to P(RO_x) among OVOC species and the contributions
320 of other OVOC species was generally smaller than that of HCHO (Tan et al., 2019a;Tan
321 et al., 2017;Tan et al., 2018;Tan et al., 2019b). In contrast, the results of this study
322 suggest that non-HCHO OVOCs have a potential to be a larger contributor than HCHO
323 and HONO, revealing the importance of non-HCHO OVOCs in radical production. The
324 difference between this study and previous studies in China is primarily attributed to
325 more OVOC species measured in this study than previous studies. The Nevertheless,
326 the existing isomers of carbonyls with more carbons lead to large uncertainties in the
327 quantification of P(RO_x) as shown in **Figure 2a**. Therefore, precise distinction of these
328 isomers in the future is crucial to accurately quantify P(RO_x). In addition, absorption
329 cross-sections and quantum yields of many photodegradable OVOC species with large
330 carbon numbers, especially multifunctional species, are not experimentally determined.
331 As a result, the photolysis frequencies of these species are not available, which also
332 leads to uncertainties in quantifying P(RO_x). As measurements of many organic
333 compounds may not be possible at least in the near future, construction of
334 parameterization method for photolysis frequencies of oxygenated VOCs either based
335 on chemical formula or functional groups at isomeric level will help to reduce this

336 uncertainty in the future.

337 As a comparison with the scenario with all observed OVOC species constrained
338 in the box model, P(RO_x) was also simulated by the box model without observed
339 OVOC species constrained. As shown in **Figure 3a**, the simulation of the box model
340 without observed OVOC species constrained (blue line in **Figure 3a**) underestimated
341 P(RO_x) significantly compared to the scenario with all observed OVOC species
342 constrained (red lines in **Figure 3a**). The underestimation of P(RO_x) was 16% and 44%
343 when using the lower and higher limits of OVOCs photolysis frequencies, respectively
344 (red solid line and red dashed line in **Figure 3a**). In this case, the underestimation of
345 OH and HO₂ concentrations was 15~38% and 25%~64%, respectively. The
346 underestimation of P(RO_x) and radical concentrations was due to the underestimation
347 of photodegradable OVOCs simulated by the photochemical model (**Table S2**). In
348 general, most photodegradable OVOCs were underestimated by 10~100% by box
349 model except for MVK and MACR. The underestimation of photodegradable OVOCs
350 can be caused by missing primary emissions (McDonald et al., 2018;Karl et al.,
351 2018;Gkatzelis et al., 2021) or unknown secondary sources of these OVOC species
352 (Bloss et al., 2005;Ji et al., 2017). Direct flux measurements of VOCs based on the eddy
353 covariance technique showed that the contribution of typical urban emission sources
354 comprised of a surprisingly large portion of OVOCs (Karl et al., 2018). In addition,
355 some experimental studies indicated that MCM mechanism generally underestimated
356 formation of aldehydes, ketones and phenols from the oxidation of aromatics by OH
357 radical (Bloss et al., 2005;Ji et al., 2017), suggesting the existence of unknown
358 secondary source of these OVOC species. This evidence suggests that it is essential to
359 use ambient measurements of OVOCs as constraints in models at least until primary
360 and secondary sources of OVOCs are better understood.

361 Previous studies in Pearl River Delta and North China Plain of China found that
362 photochemical models significantly underestimated measured concentrations of OH
363 radicals, indicating the existence of unknown sources of RO_x radicals in the atmosphere
364 (Lu et al., 2012;Lu et al., 2013;Tan et al., 2019c;Hofzumahaus et al., 2009;Ma et al.,
365 2019). For instance, comprehensive measurements in winter in Beijing showed that the

366 photochemical box model greatly underestimated OH, HO₂ and RO₂ radicals by 50%
367 ~ 12 fold during the pollution periods (Tan et al., 2018;Ma et al., 2019). Through the
368 budget analysis of the source and sink of radicals, the researchers believed that the
369 missing P(RO_x) was the primary cause of the underestimation of HO₂ and RO₂
370 concentrations (Tan et al., 2018). Given that most photodegradable OVOCs were not
371 constrained in box model used in these previous studies of RO_x radicals, the results of
372 our study provide a direction for solving this issue regarding underestimated RO_x
373 radical concentrations. Therefore, it is imperative to continuously improve
374 measurement technologies to achieve accurate quantification of more photodegradable
375 OVOC species, thereby improving our understanding of the issues with respect to the
376 closure of RO_x radicals in the atmosphere.

377 **3.3 The role of photolysis reactions in ozone pollution**

378 The box model was used to evaluate the effect of the photodegradable OVOC
379 species on ozone production rate during the whole campaign. P(O₃) were simulated
380 with and without all of measured photodegradable OVOCs species constrained in the
381 box model, respectively. As shown in **Figure 3b**, compared to the scenario with
382 observed photodegradable OVOC species constrained in box model (red lines in
383 **Figure 3b**), the scenario without constraining observed OVOCs (blue line in **Figure**
384 **3b**) underestimated peak value of P(O₃) by 15~38%. The underestimation of P(O₃)
385 was due to the underestimation of OVOCs by the box model (**Table S2**).

386 As shown in **Figure 4**, the dependence of daily peak O₃ concentrations on NO_x
387 concentrations was calculated by the box model with and without all of measured
388 photodegradable OVOC species constrained. The NO_x concentration level
389 corresponding to maximum of ozone concentration (NO_x (O₃ max)) was determined. In
390 reality, this NO_x concentration level is the threshold to distinguish between VOC-
391 limited and NO_x-limited regimes (Edwards et al., 2014;Womack et al., 2019). Ozone
392 production is NO_x-limited if the ambient NO_x concentration is lower than the
393 threshold of NO_x, but is in VOC-limited regime if ambient NO_x concentration higher
394 than the threshold of NO_x. The larger threshold of NO_x represents higher possibility

395 of ozone production in NO_x limited regime. The threshold of NO_x for the scenario
396 with observed photodegradable OVOC species constrained is 21%~52% higher than
397 that without observed photodegradable OVOC species constrained (**Figure 4**). This
398 suggests that the box model simulation without constraining OVOCs will
399 overestimate the VOC-limited degree due to the underestimation of OVOCs, and thus
400 overestimate the effect of VOCs reduction in reducing ozone pollution, which in turn
401 may not determine the ozone control strategy correctly. Therefore, it is necessary to
402 constrain these important photodegradable species in photochemical models to
403 calculate P(O₃) level and to diagnose ozone sensitivity regimes accurately.

404 O₃ production rate can be expressed as the product of P(RO_x) and radical chain
405 length (ChL) as shown in E3 (Tonnesen and Dennis, 2000).

$$406 \quad P(O_3) = P(RO_x) \times \frac{\text{Rate}(HO_2+NO)+\text{Rate}(RO_2+NO)}{P(RO_x)} = P(RO_x) \times ChL \quad E3$$

407 where Rate (HO₂+NO) and Rate (RO₂+NO) represent the reaction rates between HO₂
408 and NO and between RO₂ and NO, respectively. ChL characterizes the number of
409 iterations each RO_x radical makes prior to termination. It is equal to the ratio between
410 the radical recycling rate and primary production rate (or equivalently, termination
411 rate), indicating the efficiency of radical propagation.

412 Two ozone pollution episodes (from 19 September to 27 September and from 30
413 September to 9 October, respectively) were identified during the campaign from 14
414 September to 20 November 2018 (**Figure S6, Table S3**). The temporal variations of
415 P(O₃) and P(RO_x) overall showed good consistency with those of ozone concentrations
416 (**Figure S7**). P(O₃) in the two ozone pollution episodes was a factor of 2.6~2.8 that in
417 the non-pollution period (**Figure 5, Figure S8**). P(RO_x) in the two ozone pollution
418 episodes was a factor of 2.2~2.6 that in the non-pollution period. ChL in episode 2 was
419 similar to that in non-pollution period, while ChL for episode 1 was a factor of 1.7 that
420 in non-pollution period (**Figure S8**). Therefore, the substantial increase of P(RO_x) in
421 both ozone pollution episodes played a crucial role in the accelerated ozone production.
422 Furthermore, the ratio of P(RO_x) from OVOCs photolysis to total P(RO_x) in the two
423 ozone pollution episodes is higher than that in the non-pollution period, denoting higher

424 contribution of OVOCs photolysis to P(RO_x) in the ozone pollution episodes (**Figure**
425 **5**). These results indicate that the accelerating production of OVOCs had a significant
426 positive feedback effect on ozone pollution (Qu et al., 2021). This is broadly consistent
427 with the wintertime observations in an oil and gas basin in Utah, USA, which found
428 that a very high VOC to NO_x ratio optimized production of secondary OVOCs, leading
429 to OVOC photolysis as a dominant oxidant source (Edwards et al., 2014).

430 **4 Summary and Conclusion**

431 In summary, comprehensive measurements of photodegradable species advance
432 our understand of radical sources and ozone production in an urban environment. By
433 using PTR-ToF-MS in a representative urban environment, a large number of
434 photodegradable OVOCs were measured. These measurements make it possible to
435 directly quantify their contribution to RO_x radical production. We found that non-
436 HCHO OVOCs can be a larger contributor to P(RO_x) than HCHO and HONO.
437 Photochemical models without constrained OVOC species will significantly
438 underestimate P(RO_x) and ozone production rates and overestimate the effect of VOCs
439 reduction in reducing ozone pollution. Therefore, it is important to measure these
440 photodegradable species and use these observations as constraints to better quantify
441 radical and ozone production.

442 Thanks to the improvement of technology in the recent years, large number of
443 OVOCs species in the atmosphere can be measured by emerging online chemical
444 ionization mass spectrometers, including PTR-ToF-MS and CIMS. However,
445 photolysis frequencies of these OVOC species, especially those with multiple
446 functional groups, are still not available or difficult to quantify using current existing
447 information, which poses large uncertainties in the quantification of P(RO_x) and ozone
448 production. Hence, more laboratory studies on photolysis of organic compounds, better
449 parameterization of photolysis frequencies using chemical formula/functional groups,
450 and measurements of oxygenated VOCs at isomeric level will help to decrease this

451 uncertainty in the future.

452

453 **Data availability**

454 The observational data and model code used in this study are available from
455 corresponding authors upon request (byuan@jnu.edu.cn).

456 **Author contributions**

457 BY, WJW and HS designed the research. WJW and BY prepared the manuscript
458 with contributions from other authors. WJW performed data analysis with contributions
459 from YWP, YFC, SXY and FXB. CHW, JPQ, YBH, CMW, CSY, ZLW, BLW, XMW,
460 WS, WWH, PC, MNZ, JYZ, and MS collected data

461 **Competing interests**

462 The authors declare that they have no known competing financial interests or personal
463 relationships that could have appeared to influence the work reported in this paper.

464

465 **Acknowledgements**

466 This work was supported by the National Key R&D Plan of China (grant No.
467 2019YFE0106300), the National Natural Science Foundation of China (grant No.
468 41877302, 41905111), Guangdong Natural Science Funds for Distinguished Young
469 Scholar (grant No. 2018B030306037), Key-Area Research and Development Program
470 of Guangdong Province (grant No. 2019B110206001), Guangdong Soft Science
471 Research Program (grant No. 2019B101001005), and Guangdong Innovative and
472 Entrepreneurial Research Team Program (grant No. 2016ZT06N263). This work was
473 also supported by Special Fund Project for Science and Technology Innovation Strategy
474 of Guangdong Province (Grant No.2019B121205004).

475

476 **References:**

- 477 Atkinson, R.: Atmospheric chemistry of VOCs and NO_x, *Atmos. Environ.*, 34, 2063-
478 2101, 2000.
- 479 Bejan, I., Abd El Aal, Y., Barnes, I., Benter, T., Bohn, B., Wiesen, P., and Kleffmann, J.:
480 The photolysis of ortho-nitrophenols: a new gas phase source of HONO, *Physical*
481 *Chemistry Chemical Physics*, 8, 2028-2035, 2006.
- 482 Berges, M. G., and Warneck, P.: Product quantum yields for the 350 nm
483 photodecomposition of pyruvic acid in air, *Berichte der Bunsengesellschaft für*
484 *physikalische Chemie*, 96, 413-416, 1992.
- 485 Bloss, C., Wagner, V., Bonzanini, A., Jenkin, M. E., Wirtz, K., Martin-Reviejo, M., and
486 Pilling, M. J.: Evaluation of detailed aromatic mechanisms (MCMv3 and MCMv3.1)
487 against environmental chamber data, *Atmos. Chem. Phys.*, 5, 623-639, 10.5194/acp-5-
488 623-2005, 2005.
- 489 Burkholder, J., Sander, S., Abbatt, J., Barker, J., Cappa, C., Crouse, J., Dibble, T., Huie,
490 R., Kolb, C., and Kurylo, M.: Chemical kinetics and photochemical data for use in
491 atmospheric studies; evaluation number 19, Pasadena, CA: Jet Propulsion Laboratory,
492 National Aeronautics and Space ..., 2020.
- 493 Chen, J., Wenger, J. C., and Venables, D. S.: Near-ultraviolet absorption cross sections
494 of nitrophenols and their potential influence on tropospheric oxidation capacity, *The*
495 *Journal of Physical Chemistry A*, 115, 12235-12242, 2011.
- 496 Edwards, P. M., Brown, S. S., Roberts, J. M., Ahmadov, R., Banta, R. M., deGouw, J.
497 A., Dubé, W. P., Field, R. A., Flynn, J. H., Gilman, J. B., Graus, M., Helmig, D., Koss,
498 A., Langford, A. O., Lefer, B. L., Lerner, B. M., Li, R., Li, S.-M., McKeen, S. A.,
499 Murphy, S. M., Parrish, D. D., Senff, C. J., Soltis, J., Stutz, J., Sweeney, C., Thompson,
500 C. R., Trainer, M. K., Tsai, C., Veres, P. R., Washenfelder, R. A., Warneke, C., Wild, R.
501 J., Young, C. J., Yuan, B., and Zamora, R.: High winter ozone pollution from carbonyl
502 photolysis in an oil and gas basin, *Nature*, 514, 351-354, 10.1038/nature13767, 2014.
- 503 Ehhalt, D. H., and Rohrer, F.: Dependence of the OH concentration on solar UV, *J.*
504 *Geophys. Res.-Atmos.*, 105, 3565-3571, 10.1029/1999jd901070, 2000.
- 505 Emmerson, K. M., Carslaw, N., Carpenter, L. J., Heard, D. E., Lee, J. D., and Pilling,
506 M. J.: Urban Atmospheric Chemistry During the PUMA Campaign 1: Comparison of
507 Modelled OH and HO₂ Concentrations with Measurements, *J. Atmos. Chem.*, 52, 143-
508 164, 10.1007/s10874-005-1322-3, 2005.
- 509 Gkatzelis, G. I., Coggon, M. M., McDonald, B. C., Peischl, J., Gilman, J. B., Aikin, K.
510 C., Robinson, M. A., Canonaco, F., Prevot, A. S., and Trainer, M.: Observations confirm
511 that volatile chemical products are a major source of petrochemical emissions in US
512 cities, *Environ. Sci. Technol.*, 55, 4332-4343, 2021.
- 513 Griffith, S. M., Hansen, R., Dusanter, S., Michoud, V., Gilman, J., Kuster, W., Veres, P.,
514 Graus, M., de Gouw, J., and Roberts, J.: Measurements of hydroxyl and hydroperoxy
515 radicals during CalNex-LA: Model comparisons and radical budgets, *J. Geophys. Res.-*
516 *Atmos.*, 121, 4211-4232, 2016.
- 517 Hofzumahaus, A., Rohrer, F., Lu, K., Bohn, B., Brauers, T., Chang, C.-C., Fuchs, H.,
518 Holland, F., Kita, K., and Kondo, Y.: Amplified trace gas removal in the troposphere,

519 science, 324, 1702-1704, 2009.

520 Horowitz, A., Meller, R., and Moortgat, G. K.: The UV–VIS absorption cross sections
521 of the α -dicarbonyl compounds: pyruvic acid, biacetyl and glyoxal, *Journal of*
522 *Photochemistry and Photobiology A: Chemistry*, 146, 19-27, 2001.

523 Jenkin, M. E., Saunders, S. M., and Pilling, M. J.: The tropospheric degradation of
524 volatile organic compounds: a protocol for mechanism development, *Atmos. Environ.*,
525 31, 81-104, 1997.

526 Jenkin, M. E., Saunders, S. M., Wagner, V., and Pilling, M. J.: Protocol for the
527 development of the Master Chemical Mechanism, MCM v3 (Part B): tropospheric
528 degradation of aromatic volatile organic compounds, *Atmos. Chem. Phys.*, 3, 181-193,
529 10.5194/acp-3-181-2003, 2003.

530 Ji, Y., Zhao, J., Terazono, H., Misawa, K., Levitt, N. P., Li, Y., Lin, Y., Peng, J., Wang,
531 Y., Duan, L., Pan, B., Zhang, F., Feng, X., An, T., Marrero-Ortiz, W., Secret, J., Zhang,
532 A. L., Shibuya, K., Molina, M. J., and Zhang, R.: Reassessing the atmospheric oxidation
533 mechanism of toluene, *Proc. National Acad. Sci.*, 114, 8169-8174,
534 10.1073/pnas.1705463114, 2017.

535 Karl, T., Striednig, M., Graus, M., Hammerle, A., and Wohlfahrt, G.: Urban flux
536 measurements reveal a large pool of oxygenated volatile organic compound emissions,
537 *Proc. National Acad. Sci.*, 115, 1186-1191, 2018.

538 Lelieveld, J., Butler, T. M., Crowley, J. N., Dillon, T. J., Fischer, H., Ganzeveld, L.,
539 Harder, H., Lawrence, M. G., Martinez, M., Taraborrelli, D., and Williams, J.:
540 Atmospheric oxidation capacity sustained by a tropical forest, *Nature*, 452, 737-740,
541 10.1038/nature06870, 2008.

542 Li, K., Jacob, D. J., Liao, H., Qiu, Y., Shen, L., Zhai, S., Bates, K. H., Sulprizio, M. P.,
543 Song, S., and Lu, X.: Ozone pollution in the North China Plain spreading into the late-
544 winter haze season, *Proc. National Acad. Sci.*, 118, 2021.

545 Li, X., Rohrer, F., Brauers, T., Hofzumahaus, A., Lu, K., Shao, M., Zhang, Y. H., and
546 Wahner, A.: Modeling of HCHO and CHOCHO at a semi-rural site in southern China
547 during the PRIDE-PRD2006 campaign, *Atmos. Chem. Phys.*, 14, 12291-12305,
548 10.5194/acp-14-12291-2014, 2014.

549 Ling, Z., Guo, H., Lam, S., Saunders, S., and Wang, T.: Atmospheric photochemical
550 reactivity and ozone production at two sites in Hong Kong: Application of a master
551 chemical mechanism–photochemical box model, *J. Geophys. Res.-Atmos.*, 119, 10567-
552 10582, 2014.

553 Lu, K., Rohrer, F., Holland, F., Fuchs, H., Bohn, B., Brauers, T., Chang, C., Häsel, R.,
554 Hu, M., and Kita, K.: Observation and modelling of OH and HO₂ concentrations in the
555 Pearl River Delta 2006: a missing OH source in a VOC rich atmosphere, *Atmos. Chem.*
556 *Phys.*, 12, 1541, 2012.

557 Lu, K. D., Hofzumahaus, A., Holland, F., Bohn, B., Brauers, T., Fuchs, H., Hu, M.,
558 Haseler, R., Kita, K., Kondo, Y., Li, X., Lou, S. R., Oebel, A., Shao, M., Zeng, L. M.,
559 Wahner, A., Zhu, T., Zhang, Y. H., and Rohrer, F.: Missing OH source in a suburban
560 environment near Beijing: observed and modelled OH and HO₂ concentrations in
561 summer 2006, *Atmospheric Chemistry and Physics*, 13, 1057-1080, 10.5194/acp-13-
562 1057-2013, 2013.

563 Ma, X., Tan, Z., Lu, K., Yang, X., Liu, Y., Li, S., Li, X., Chen, S., Novelli, A., and Cho,
564 C.: Winter photochemistry in Beijing: Observation and model simulation of OH and
565 HO₂ radicals at an urban site, *Sci. Total Environ.*, 685, 85-95, 2019.

566 McDonald, B. C., De Gouw, J. A., Gilman, J. B., Jathar, S. H., Akherati, A., Cappa, C.
567 D., Jimenez, J. L., Lee-Taylor, J., Hayes, P. L., and McKeen, S. A.: Volatile chemical
568 products emerging as largest petrochemical source of urban organic emissions, *Science*,
569 359, 760-764, 2018.

570 Mellouki, A., and Mu, Y.: On the atmospheric degradation of pyruvic acid in the gas
571 phase, *Journal of Photochemistry and Photobiology A: Chemistry*, 157, 295-300, 2003.

572 Monks, P. S., Archibald, A., Colette, A., Cooper, O., Coyle, M., Derwent, R., Fowler,
573 D., Granier, C., Law, K. S., and Mills, G.: Tropospheric ozone and its precursors from
574 the urban to the global scale from air quality to short-lived climate forcer, *Atmos. Chem.*
575 *Phys.*, 15, 8889-8973, 2015.

576 Qu, H., Wang, Y., Zhang, R., Liu, X., Huey, L. G., Sjostedt, S., Zeng, L., Lu, K., Wu,
577 Y., and Shao, M.: Chemical Production of Oxygenated Volatile Organic Compounds
578 Strongly Enhances Boundary-Layer Oxidation Chemistry and Ozone Production,
579 *Environ. Sci. Technol.*, 55, 13718-13727, 2021.

580 Rohrer, F., Lu, K., Hofzumahaus, A., Bohn, B., Brauers, T., Chang, C.-C., Fuchs, H.,
581 Häsel, R., Holland, F., and Hu, M.: Maximum efficiency in the hydroxyl-radical-
582 based self-cleansing of the troposphere, *Nat. Geosci.*, 7, 559-563, 2014a.

583 Rohrer, F., Lu, K., Hofzumahaus, A., Bohn, B., Brauers, T., Chang, C.-C., Fuchs, H.,
584 Häsel, R., Holland, F., Hu, M., Kita, K., Kondo, Y., Li, X., Lou, S., Oebel, A., Shao,
585 M., Zeng, L., Zhu, T., Zhang, Y., and Wahner, A.: Maximum efficiency in the hydroxyl-
586 radical-based self-cleansing of the troposphere, *Nature Geoscience*, 7, 559-563,
587 10.1038/ngeo2199, 2014b.

588 Sangwan, M., and Zhu, L.: Role of methyl-2-nitrophenol photolysis as a potential
589 source of OH radicals in the polluted atmosphere: implications from laboratory
590 investigation, *The Journal of Physical Chemistry A*, 122, 1861-1872, 2018.

591 Saunders, S. M., Jenkin, M. E., Derwent, R., and Pilling, M.: Protocol for the
592 development of the Master Chemical Mechanism, MCM v3 (Part A): tropospheric
593 degradation of non-aromatic volatile organic compounds, 2003.

594 Sekimoto, K., Li, S.-M., Yuan, B., Koss, A., Coggon, M., Warneke, C., and de Gouw,
595 J.: Calculation of the sensitivity of proton-transfer-reaction mass spectrometry (PTR-
596 MS) for organic trace gases using molecular properties, *International Journal of Mass*
597 *Spectrometry*, 421, 71-94, 10.1016/j.ijms.2017.04.006, 2017.

598 Sheehy, P. M., Volkamer, R., Molina, L. T., and Molina, M. J.: Oxidative capacity of
599 the Mexico City atmosphere - Part 2: A RO_x radical cycling perspective, *Atmos. Chem.*
600 *Phys.*, 10, 6993-7008, 10.5194/acp-10-6993-2010, 2010.

601 Sinha, V., Williams, J., Crowley, J. N., and Lelieveld, J.: The Comparative Reactivity
602 Method – a new tool to measure total OH Reactivity in ambient air, *Atmos.*
603 *Chem. Phys.*, 8, 2213-2227, 10.5194/acp-8-2213-2008, 2008.

604 Stone, D., Whalley, L. K., and Heard, D. E.: Tropospheric OH and HO₂ radicals: field
605 measurements and model comparisons, *Chemical Society Reviews*, 41, 6348-6404,
606 10.1039/c2cs35140d, 2012.

607 Tan, Z., Fuchs, H., Lu, K., Hofzumahaus, A., Bohn, B., Broch, S., Dong, H., Gomm, S.,
608 Häsel, R., He, L., Holland, F., Li, X., Liu, Y., Lu, S., Rohrer, F., Shao, M., Wang, B.,
609 Wang, M., Wu, Y., Zeng, L., Zhang, Y., Wahner, A., and Zhang, Y.: Radical chemistry
610 at a rural site (Wangdu) in the North China Plain: observation and model calculations
611 of OH, HO₂ and RO₂ radicals, *Atmos. Chem. Phys.*, 17, 663-690, 10.5194/acp-17-663-
612 2017, 2017.

613 Tan, Z., Rohrer, F., Lu, K., Ma, X., Bohn, B., Broch, S., Dong, H., Fuchs, H., Gkatzelis,
614 G. I., Hofzumahaus, A., Holland, F., Li, X., Liu, Y., Liu, Y., Novelli, A., Shao, M., Wang,
615 H., Wu, Y., Zeng, L., Hu, M., Kiendler-Scharr, A., Wahner, A., and Zhang, Y.:
616 Wintertime photochemistry in Beijing: observations of RO_x radical concentrations in
617 the North China Plain during the BEST-ONE campaign, *Atmos. Chem. Phys.*, 18,
618 12391-12411, 10.5194/acp-18-12391-2018, 2018.

619 Tan, Z., Lu, K., Hofzumahaus, A., Fuchs, H., Bohn, B., Holland, F., Liu, Y., Rohrer, F.,
620 Shao, M., and Sun, K.: Experimental budgets of OH, HO₂, and RO₂ radicals and
621 implications for ozone formation in the Pearl River Delta in China 2014, *Atmos. Chem.*
622 *Phys.*, 19, 7129-7150, 2019a.

623 Tan, Z., Lu, K., Jiang, M., Su, R., Wang, H., Lou, S., Fu, Q., Zhai, C., Tan, Q., Yue, D.,
624 Chen, D., Wang, Z., Xie, S., Zeng, L., and Zhang, Y.: Daytime atmospheric oxidation
625 capacity in four Chinese megacities during the photochemically polluted season: a case
626 study based on box model simulation, *Atmos. Chem. Phys.*, 19, 3493-3513,
627 10.5194/acp-19-3493-2019, 2019b.

628 Tan, Z. F., Lu, K. D., Hofzumahaus, A., Fuchs, H., Bohn, B., Holland, F., Liu, Y. H.,
629 Rohrer, F., Shao, M., Sun, K., Wu, Y. S., Zeng, L. M., Zhang, Y. S., Zou, Q., Kiendler-
630 Scharr, A., Wahner, A., and Zhang, Y. H.: Experimental budgets of OH, HO₂, and RO₂
631 radicals and implications for ozone formation in the Pearl River Delta in China 2014,
632 *Atmos. Chem. Phys.*, 19, 7129-7150, 10.5194/acp-19-7129-2019, 2019c.

633 Tonnesen, G. S., and Dennis, R. L.: Analysis of radical propagation efficiency to assess
634 ozone sensitivity to hydrocarbons and NO_x: 1. Local indicators of instantaneous odd
635 oxygen production sensitivity, *J. Geophys. Res.-Atmos.*, 105, 9213-9225, 2000.

636 Volkamer, R., Sheehy, P., Molina, L. T., and Molina, M. J.: Oxidative capacity of the
637 Mexico City atmosphere - Part 1: A radical source perspective, *Atmos. Chem. Phys.*,
638 10, 6969-6991, 10.5194/acp-10-6969-2010, 2010.

639 Wang, C., Yuan, B., Wu, C., Wang, S., Qi, J., Wang, B., Wang, Z., Hu, W., Chen, W.,
640 Ye, C., Wang, W., Sun, Y., Wang, C., Huang, S., Song, W., Wang, X., Yang, S., Zhang,
641 S., Xu, W., Ma, N., Zhang, Z., Jiang, B., Su, H., Cheng, Y., Wang, X., and Shao, M.:
642 Measurements of higher alkanes using NO⁺ chemical ionization in PTR-ToF-MS:
643 important contributions of higher alkanes to secondary organic aerosols in China,
644 *Atmospheric Chemistry and Physics*, 20, 14123-14138, 10.5194/acp-20-14123-2020,
645 2020a.

646 Wang, W., Li, X., Shao, M., Hu, M., Zeng, L., Wu, Y., and Tan, T.: The impact of
647 aerosols on photolysis frequencies and ozone production in Beijing during the 4-year
648 period 2012–2015, *Atmos. Chem. Phys.*, 19, 9413-9429, 10.5194/acp-19-9413-2019,
649 2019.

650 Wang, W., Parrish, D. D., Li, X., Shao, M., Liu, Y., Mo, Z., Lu, S., Hu, M., Fang, X.,

651 and Wu, Y.: Exploring the drivers of the increased ozone production in Beijing in
652 summertime during 2005–2016, *Atmos. Chem. Phys.*, 20, 15617-15633, 2020b.

653 Wang, W., Parrish, D. D. P., Li, X., Shao, M., Liu, Y., Lu, S., Hu, M., Wu, Y., Zeng, L.,
654 and Zhang, Y.: Exploring the drivers of the elevated ozone production in Beijing in
655 summertime during 2005–2016, *Atmospheric Chemistry and Physics Discussions*, 1-
656 40, 2020c.

657 Wang, W., Li, X., Kuang, Y., Su, H., Cheng, Y., Hu, M., Zeng, L., Tan, T., and Zhang,
658 Y.: Exploring the Drivers and Photochemical Impact of the Positive Correlation
659 between Single Scattering Albedo and Aerosol Optical Depth in the Troposphere,
660 *Environ. Sci. Technol. Lett.*, 2021a.

661 Wang, W., Qi, J., Zhou, J., Yuan, B., Peng, Y., Wang, S., Yang, S., Williams, J., Sinha,
662 V., and Shao, M.: The improved comparative reactivity method (ICRM): measurements
663 of OH reactivity under high-NO_x conditions in ambient air, *Atmos. Meas. Tech.*, 14,
664 2285-2298, 2021b.

665 Womack, C. C., McDuffie, E. E., Edwards, P. M., Bares, R., de Gouw, J. A., Docherty,
666 K. S., Dubé, W. P., Fibiger, D. L., Franchin, A., Gilman, J. B., Goldberger, L., Lee, B.
667 H., Lin, J. C., Long, R., Middlebrook, A. M., Millet, D. B., Moravek, A., Murphy, J. G.,
668 Quinn, P. K., Riedel, T. P., Roberts, J. M., Thornton, J. A., Valin, L. C., Veres, P. R.,
669 Whitehill, A. R., Wild, R. J., Warneke, C., Yuan, B., Baasandorj, M., and Brown, S. S.:
670 An Odd Oxygen Framework for Wintertime Ammonium Nitrate Aerosol Pollution in
671 Urban Areas: NO_x and VOC Control as Mitigation Strategies, *Geophys. Res. Lett.*, 46,
672 4971-4979, 10.1029/2019gl082028, 2019.

673 Wu, C., Wang, C., Wang, S., Wang, W., Yuan, B., Qi, J., Wang, B., Wang, H., Wang, C.,
674 Song, W., Wang, X., Hu, W., Lou, S., Ye, C., Peng, Y., Wang, Z., Huangfu, Y., Xie, Y.,
675 Zhu, M., Zheng, J., Wang, X., Jiang, B., Zhang, Z., and Shao, M.: Measurement report:
676 Important contributions of oxygenated compounds to emissions and chemistry of
677 volatile organic compounds in urban air, *Atmospheric Chemistry and Physics*, 20,
678 14769-14785, 10.5194/acp-20-14769-2020, 2020.

679 Ye, C., Yuan, B., Lin, Y., Wang, Z., Hu, W., Li, T., Chen, W., Wu, C., Wang, C., Huang,
680 S., Qi, J., Wang, B., Wang, C., Song, W., Wang, X., Zheng, E., Krechmer, J. E., Ye, P.,
681 Zhang, Z., Wang, X., Worsnop, D. R., and Shao, M.: Chemical characterization of
682 oxygenated organic compounds in the gas phase and particle phase using iodide CIMS
683 with FIGAERO in urban air, *Atmospheric Chemistry and Physics*, 21, 8455-8478,
684 10.5194/acp-21-8455-2021, 2021.

685 Young, C. J., Washenfelder, R. A., Roberts, J. M., Mielke, L. H., Osthoff, H. D., Tsai,
686 C., Pikelnaya, O., Stutz, J., Veres, P. R., and Cochran, A. K.: Vertically resolved
687 measurements of nighttime radical reservoirs in Los Angeles and their contribution to
688 the urban radical budget, *Environ. Sci. Technol.*, 46, 10965-10973, 2012.

689 Yu, Y., Cheng, P., Li, H., Yang, W., Han, B., Song, W., Hu, W., Wang, X., Yuan, B.,
690 Shao, M., Huang, Z., Li, Z., Zheng, J., Wang, H., and Yu, X.: Budget of nitrous acid
691 (HONO) and its impacts on atmospheric oxidation capacity at an urban site in the fall
692 season of Guangzhou, China, *Atmos. Chem. Phys. Discuss.*, 2021, 1-38, 10.5194/acp-
693 2021-178, 2021.

694 Yuan, B., Liggio, J., Wentzell, J., Li, S. M., Stark, H., Roberts, J. M., Gilman, J., Lerner,

695 B., Warneke, C., Li, R., Leithead, A., Osthoff, H. D., Wild, R., Brown, S. S., and de
696 Gouw, J. A.: Secondary formation of nitrated phenols: insights from observations
697 during the Uintah Basin Winter Ozone Study (UBWOS) 2014, *Atmos. Chem. Phys.*, 16,
698 2139-2153, 10.5194/acp-16-2139-2016, 2016.

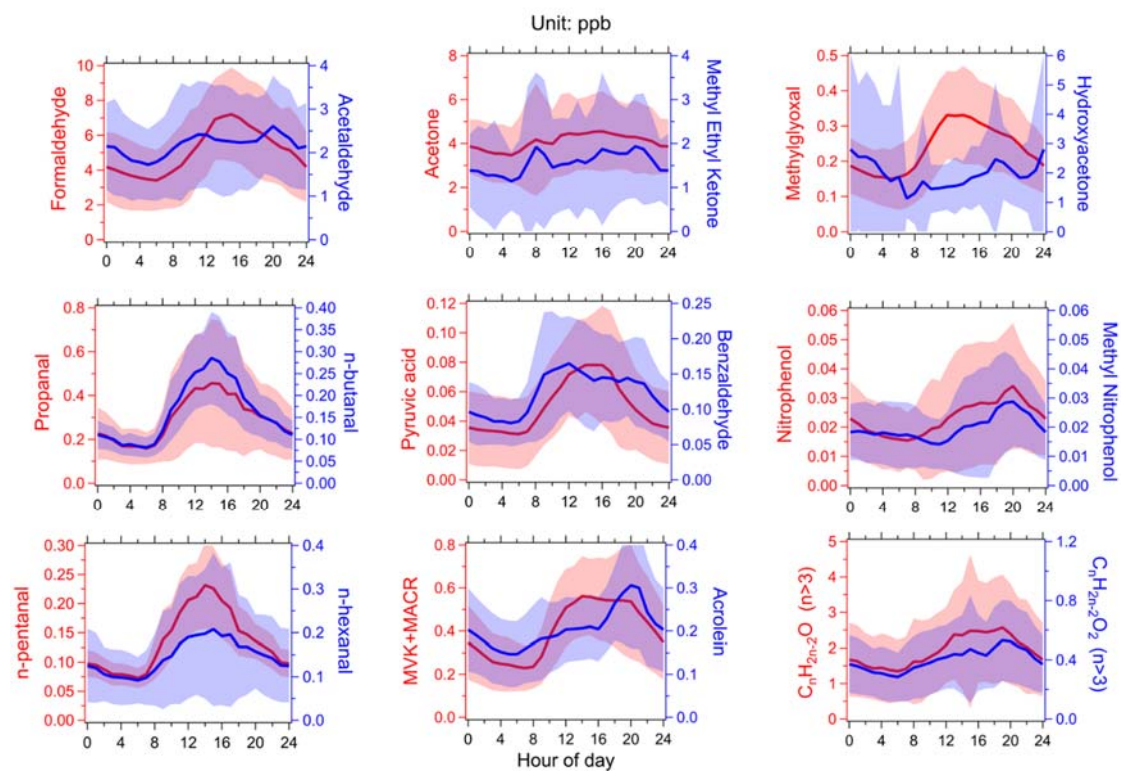
699 Yuan, B., Koss, A. R., Warneke, C., Coggon, M., Sekimoto, K., and de Gouw, J. A.:
700 Proton-Transfer-Reaction Mass Spectrometry: Applications in Atmospheric Sciences,
701 *Chemical Reviews*, 117, 13187-13229, 10.1021/acs.chemrev.7b00325, 2017.

702

703

704

705



706

707 Figure 1. The average diurnal variations of the concentrations of photodegradable

708 OVOCs species during the field campaign in Guangzhou. Lines and shading represent

709 averages and standard deviations, respectively.

710

711

712
 713
 714
 715
 716
 717
 718
 719
 720
 721
 722
 723
 724
 725
 726
 727
 728
 729
 730
 731
 732
 733
 734
 735
 736
 737
 738
 739
 740
 741

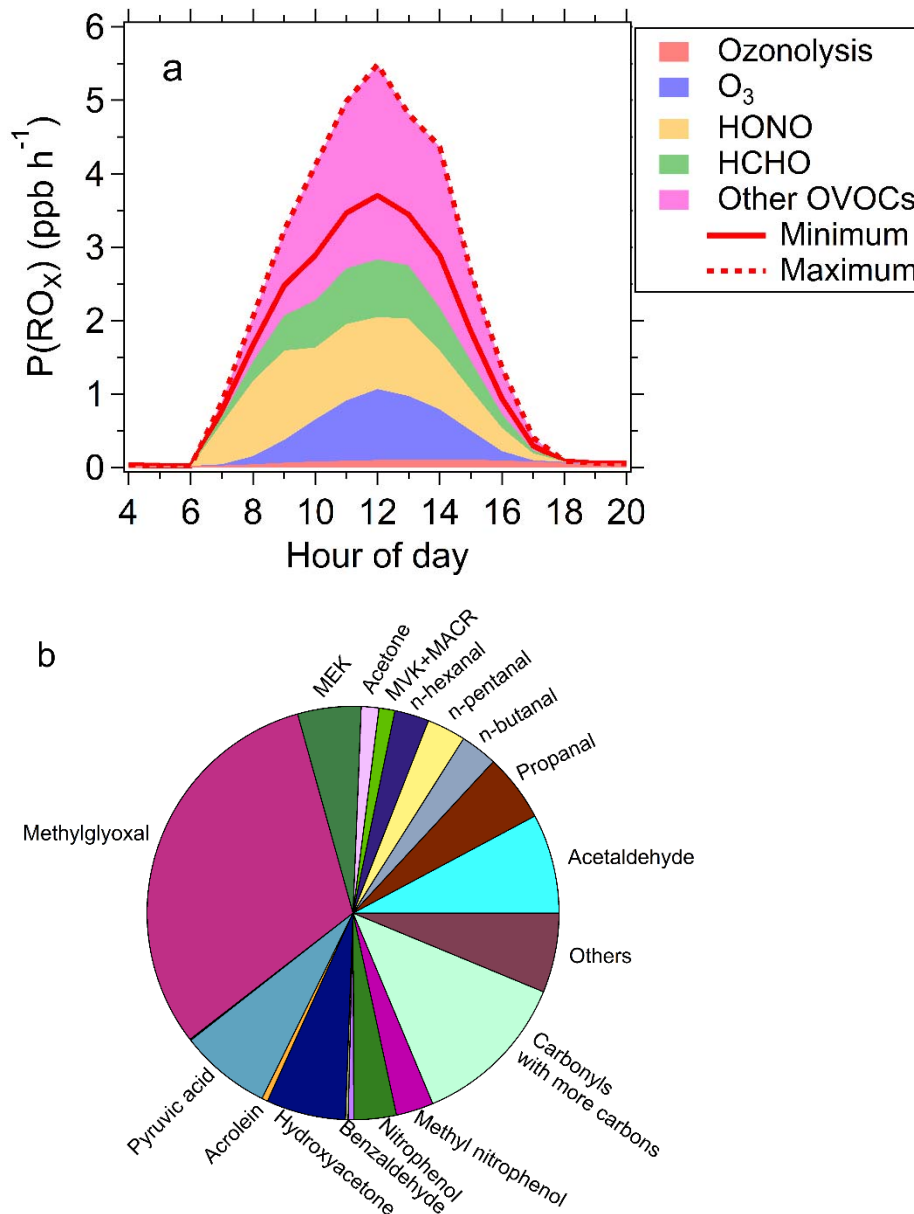


Figure 2. The P(RO_x) calculated by box model with all observed photodegradable species constrained. (a): The source composition of total P(RO_x) during the campaign; the solid and dashed lines represent the scenarios with minimum and maximum OVOC contributions to P(RO_x), respectively. (b): the relative contributions of non-HCHO OVOC species to P(RO_x) for the scenarios with minimum OVOC contribution to P(RO_x).

742
743
744
745
746
747
748
749
750
751
752
753
754
755
756
757
758
759
760
761
762
763

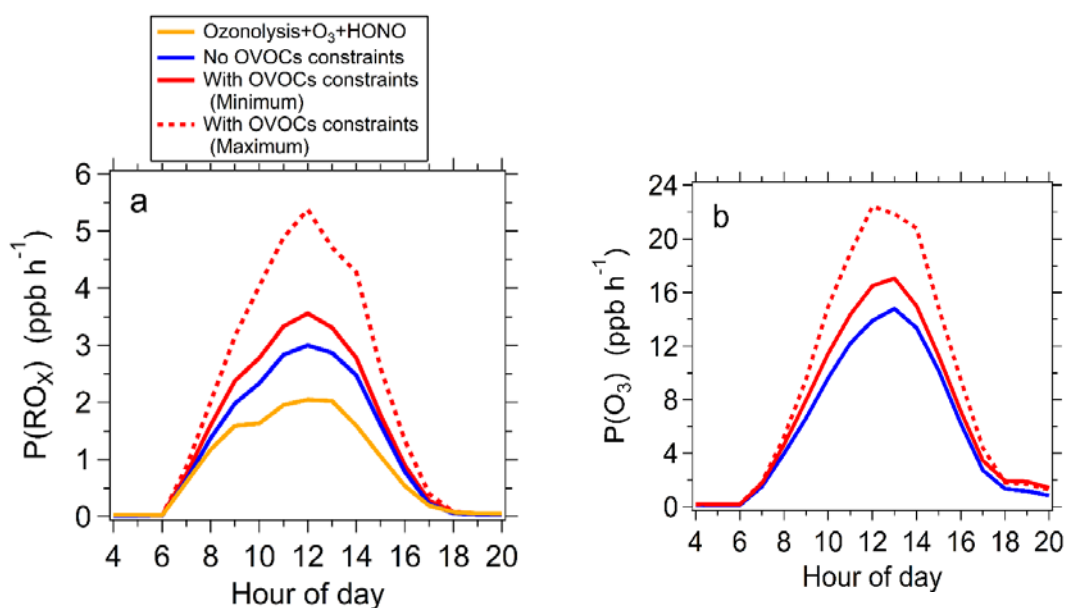
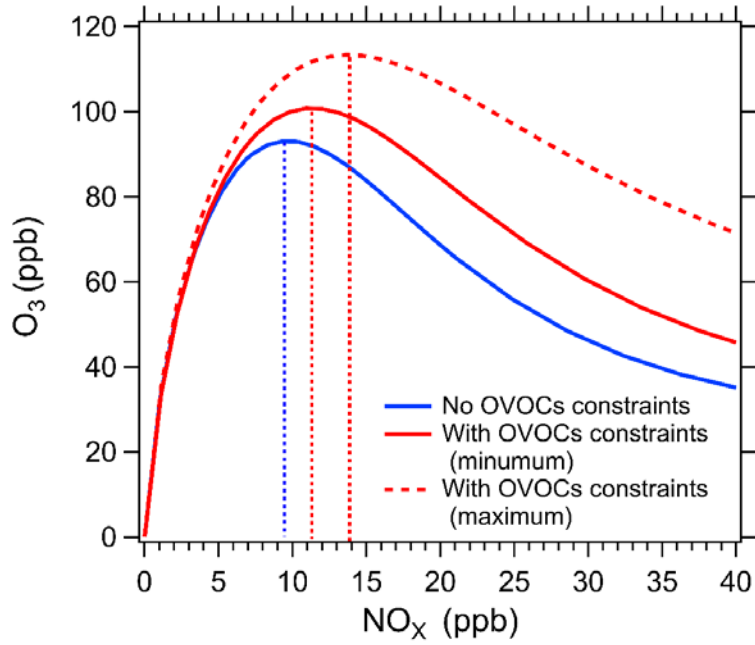


Figure 3. Model simulated $P(\text{RO}_x)$ (a) and $P(\text{O}_3)$ (b) without and with all observed photodegradable OVOCs constrained. (a): Model simulated $P(\text{RO}_x)$ without (blue line) and with all observed photodegradable OVOCs constrained (red lines). The sum contribution of O_3 photolysis, HONO photolysis and ozonolysis is also displayed (yellow line). (b): Model simulated $P(\text{O}_3)$ without (blue line) and with observed photodegradable OVOCs constrained (red lines). The red solid and red dashed lines represent the scenarios with minimum and maximum OVOC contributions to $P(\text{RO}_x)$, respectively.



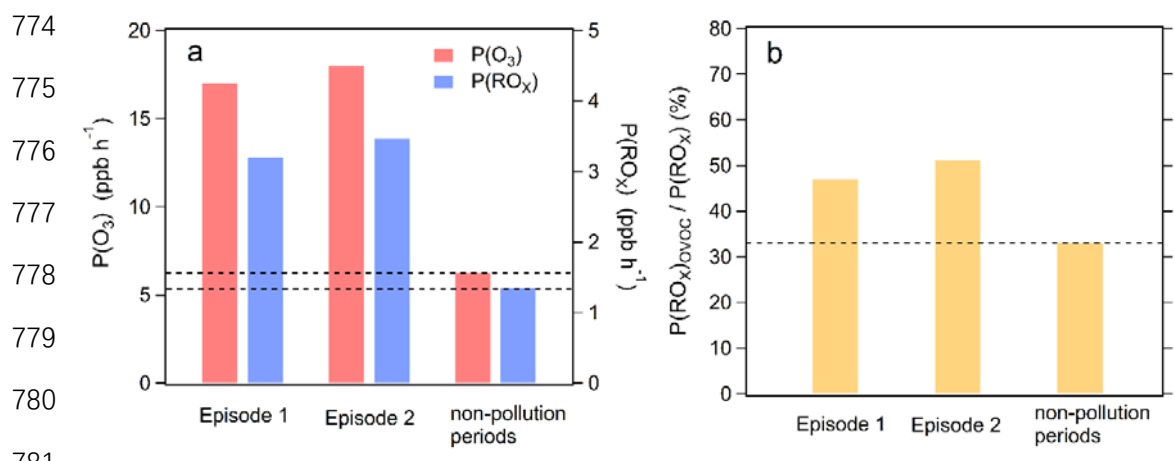
764

765 Figure 4. Model simulated dependence of daily peak O₃ concentrations on NO_x
 766 concentrations without (blue curve) and with all observed photodegradable OVOCs
 767 constrained (red curves). The red solid and red dashed curves represent the scenarios
 768 with minimum and maximum OVOC contributions to P(RO_x), respectively. The dashed
 769 lines parallel to Y-axis represent the threshold of NO_x levels to distinguish between
 770 VOC-limited and NO_x-limited regimes.

771

772

773



782 Figure 5. Averaged $P(O_3)$, $P(RO_x)$, the ratio of $P(RO_x)$ contributed by OVOCs to total
 783 $P(RO_x)$ ($P(RO_x)_{OVOC}/P(RO_x)$) during two ozone pollution episodes (episode 1,
 784 episode 2) and non-pollution periods. Both $P(O_3)$ and $P(RO_x)$ correspond to the
 785 scenarios with minimum OVOC contributions to $P(RO_x)$.

786
 787
 788